Machine-Designed Sensor to Make Optimal Use of Entanglement-Generating Dynamics for Quantum Sensing

Simon A. Haine* and Joseph J. Hope
Department of Quantum Science, Research School of Physics, Australian National University, Canberra, ACT 0200, Australia

(Received 13 September 2019; accepted 29 January 2020; published 14 February 2020)

We use machine optimization to develop a quantum sensing scheme that achieves significantly better sensitivity than traditional schemes with the same quantum resources. Utilizing one-axis twisting dynamics to generate quantum entanglement, we find that, rather than dividing the temporal resources into separate "state-preparation" and "interrogation" stages, a complicated machine-designed sequence of rotations allows for the generation of metrologically useful entanglement while the parameter is interrogated. This provides much higher sensitivities for a given total time compared to states generated via traditional one-axis twisting schemes. This approach could be applied to other methods of generating quantum-enhanced states, allowing for atomic clocks, magnetometers, and inertial sensors with increased sensitivities.

DOI: 10.1103/PhysRevLett.124.060402

Atom interferometry is a crucial technique for enabling ultrastable clocks, magnetometers, and inertial sensors [1]. In the continued push for increased sensitivity of these devices, there is considerable recent interest in the development of atom interferometry that exploits quantum entanglement to surpass the shot-noise limit (SNL) [2,3]. The large dimensionality of quantum Hilbert spaces means that even relatively simple quantum systems can display remarkably complicated dynamics. Physicists are very good at using intuition to find regimes that display simple behavior within this complexity. Quantum sensors are usually designed accordingly, ensuring that the dynamics follows simple models, and the parameter of interest is robustly correlated with a simple output signal in a way that is easily interpreted. These constraints do not necessarily maximize sensitivity, however. If we relax these design constraints, it may be possible to use machine-based optimization [4] to design sensors with superior sensitivity and robustness.

One-axis twisting (OAT) has been shown to produce spin-squeezed states capable of sub-SNL sensitivities [5–15]. However, one common criticism of this approach, or any approach that involves the preparation of quantum-enhanced states, is that the time taken to prepare these states would be better utilized interrogating the parameter of interest. That is, instead of spending time τ_{prep} preparing an entangled quantum state, and time τ_{int} using this state to interrogate the system, it would be better to devote the full time period $T = \tau_{\mathrm{prep}} + \tau_{\mathrm{int}}$ to interrogation, thus increasing the sensitivity via simply accruing a greater phase shift. Here, we consider how the use of state-preparation and interrogation *concurrently* affects the performance of the sensor. In particular, we find that OAT dynamics, combined with a complicated sequence of rotations found by machine optimization, can provide significantly better sensitivities than sensing with traditional schemes.

Model.—We assume a system of N bosons distributed among two modes (annihilation operators $\hat{a}$ and $\hat{b}$). Such a system is conveniently described by the pseudospin SU(2) algebra: $\hat{J}_k = \frac{1}{2}\mathbf{a}^\dagger \sigma_k \mathbf{a}$, where $\mathbf{a} = (\hat{a}, \hat{b})^T$, and σ_k is the kth Pauli-spin matrix. These operators obey the usual angular momentum commutation relations: $[\hat{J}_i, \hat{J}_j] = i\sum_k \epsilon_{ijk}\hat{J}_k$, where ϵ_{ijk} is the Levi-Civita symbol [16]. A general pure state can be expressed as $|\Psi\rangle = \sum_{m=-N/2}^{N/2} c_m |m\rangle$, where the state $|m\rangle \equiv |(N/2)+m, (N/2)-m\rangle$ denotes $(N/2)+m$ particles in mode a and $(N/2)-m$ particles in mode b, and is an eigenstate of $\hat{J}_z$ with eigenvalue m. We assume that the metrological parameter ω (for example, a frequency shift caused by a magnetic field) causes a rotation around the $\hat{J}_z$ axis and that the particles are interacting via a $\hat{J}_z^2$ interaction, the magnitude of which is constant in time. Additionally, we assume that we can implement an arbitrary time-dependent rotation around the $\hat{J}_x$ axis [rotation rate $\Omega(t)$], such that the Hamiltonian is

$$\hat{H} = \hbar\chi\hat{J}_z^2 + \hbar\omega\hat{J}_z + \hbar\Omega(t)\hat{J}_x. \tag{1}$$

The $\hat{J}_z^2$ term is the source of the entanglement generation in OAT dynamics [17–19], and the presence of a constant, nonzero $\hat{J}_x$ term results in "twist-and-turn" (TNT) dynamics, which has been shown to create entanglement more rapidly than OAT [20–24]. For an initial pure state $|\Psi_0\rangle$ evolving under this Hamiltonian for some duration T, the precision to which the parameter ω can be estimated by making measurements on the final state $|\Psi(T)\rangle$ is bounded by $(\Delta\omega)^2 \geq (1/F_Q)$, where F_Q is the quantum Fisher information (QFI) [25,26], given by

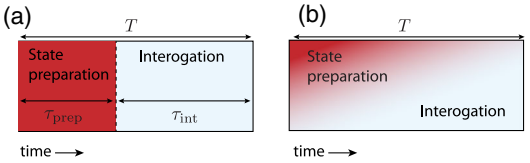

FIG. 1. (a) Traditional OAT scheme. With total available time T, time τ_{prep} is devoted to preparing the quantum state, while $\tau_{int} = T - \tau_{prep}$ is devoted to interrogating the system. (b) Machine-designed scheme customized to maximize the sensitivity, which includes dynamics which can not be separately classified as state-preparation and interrogation.

$$F_Q = 4[\langle \partial_\omega \Psi(T) | \partial_\omega \Psi(T) \rangle - |\langle \Psi(T) | \partial_\omega \Psi(T) \rangle|^2]. \quad (2)$$

It was shown in [27] that, as long as the initial state is an eigenstate of the $\hat{J}_x$ parity operator (such as a $\hat{J}_x$ eigenstate, for example), a measurement that projects into the $\hat{J}_x$ basis will saturate the quantum Cramer-Rao bound, implying that we obtain the sensitivity $\Delta\omega^2 = 1/F_Q$. With $\Omega(t) = 0$, it is straightforward to show that

$$F_Q = f_0 T^2, \quad (3)$$

where

$$f_0 = 4\mathrm{var}(\hat{J}_z) \quad (4)$$

is the QFI for sensing an instantaneously encoded phase ϕ by making measurements on the state $|\Psi_\phi\rangle = \exp(i\phi\hat{J}_z)|\Psi\rangle$. Assuming an initial state with no interparticle entanglement [i.e., a coherent spin state (CSS) [28]], the maximum possible value is $f_0 = N$, or $F_Q = NT^2$ [17,18], which we define as the shot-noise limit. In the absence of the $\hat{J}_x$ rotation, the entanglement generated by the $\hat{J}_z^2$ term does nothing to increase the sensitivity, as $\mathrm{var}(\hat{J}_z)$, and therefore f_0, are conserved. In this Letter, we investigate the optimal form of $\Omega(t)$ to maximize the sensitivity at time T. We begin by optimizing the traditional OAT scheme, where a single rotation is used to increase f_0 at some time, and then use machine optimization to consider far more general forms of $\Omega(t)$.

Optimization of traditional OAT scheme.—OAT dynamics is usually discussed in the context of spin squeezing [29], where the nonlinear interaction is used to create a state with reduced variance of the pseudospin operator along one direction. However, we will explain this process in the more general terms of QFI. In this protocol, at $t = 0$ the state is prepared in a maximum $\hat{J}_x$ eigenstate: $|\Psi_0\rangle = \exp[i(\pi/2)\hat{J}_y]|N/2\rangle$, which evolves under Eq. (1). The $\hat{J}_z^2$ interaction causes a *shearing* of the initial CSS, which increases $\mathrm{var}(\hat{J}_y)$, while $\mathrm{var}(\hat{J}_z)$ (and therefore f_0) are unaffected. In order to convert this entanglement into meteorologically useful entanglement (i.e., increasing f_0), a rotation of angle θ_0 is implemented around the $\hat{J}_x$ axis at $t = \tau_{prep}$ to convert this large $\mathrm{var}(\hat{J}_y)$ into a large f_0, such that the sensitivity of the state to the parameter ω for the remaining time $\tau_{int} = T - \tau_{prep}$ is significantly increased. This is done by choosing $\Omega(t) = \theta_0\delta(t - \tau_{prep})$, with $0 < \tau_{prep} < T$ (Fig. 1) [30]. Although the parameter ω is being interrogated for the entire duration, f_0 significantly increases at $t = \tau_{prep}$, and then remains constant thereafter, so the notion of separate state-preparation and interrogation periods remains useful. Figure 2 shows $f_0(t)$, $F_Q(t)$, and the evolution of the state generated via this scheme. The parameters τ_{prep} and θ_0 were chosen to maximize $F_Q(T)$ for the particular value of χT. The use of OAT state-preparation dynamics concurrently with interrogation was also recently considered by Hayes *et al.* [31] in a slightly different scheme. After time τ_{prep}, the $\hat{J}_z^2$ term was switched off, and an *echo* was performed by reversing the sign of the $\hat{J}_z^2$ term at time $T - \tau_{prep}$ to reverse the initial state-preparation dynamics. We found that we could obtain significantly better sensitivity without this echo and by optimizing over θ_0 [32].

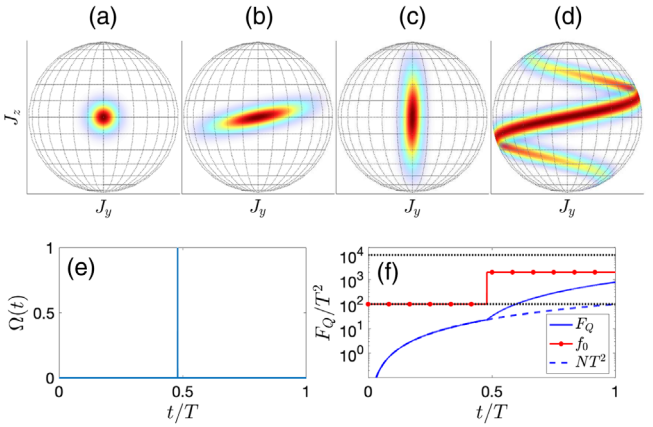

FIG. 2. Performance of the traditional OAT scheme. (a)–(d) The Husimi-Q function at (a) $t = 0$, (b) $t = \tau_{prep}$ before the rotation is applied, (c) $t = \tau_{prep}$ after the rotation $\exp(i\theta_0\hat{J}_x)$ is applied, and (d) $t = T$. (e) $\Omega(t)$. In this case, we chose $\Omega(t) = \theta_0\delta(t - \tau_{prep})$, resulting in an instantaneous rotation of magnitude θ_0. (f) $F_Q(t)/T^2$ (blue solid line) and f_0 (red circles). $F_Q(t) = Nt^2$ for an unentangled system is represented by the blue dashed line. The shot-noise limit ($f_0 = N$) and Heisenberg limit ($f_0 = N^2$) are represented by the lower and upper black dotted lines, respectively. Parameters: $N = 100$, $\chi T = 0.1$. The parameters $\theta_0 = -1.35$ and $\tau_{prep} = 0.48$ where chosen to maximize $F_Q(T)$. The Husimi-Q function is defined by $Q(\theta,\phi) = |\langle\alpha(\theta,\phi)|\Psi\rangle|^2$, where $|\alpha(\theta,\phi)\rangle$ is a coherent spin state formed by rotating the maximal $\hat{J}_z$ eigenstate: $|\alpha(\theta,\phi)\rangle = \exp(i\phi\hat{J}_z)\exp(i\theta\hat{J}_y)|N/2\rangle$.

Machine-designed scheme.—The parameter $\Omega(t)$ can be manipulated with a high degree of control, for example, by adjusting the strength of an electromagnetic field.

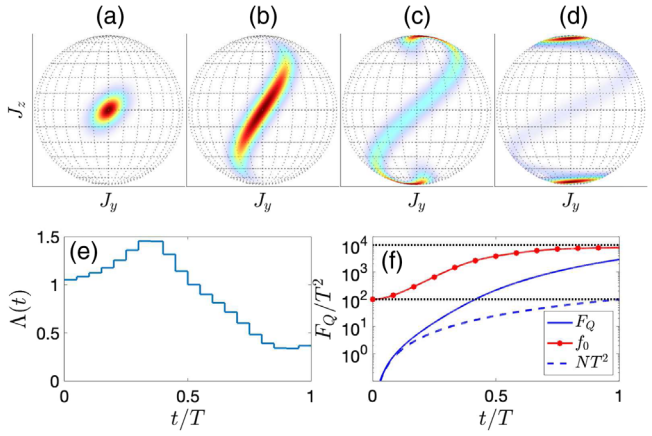

FIG. 3. Performance of the machine-designed scheme. (a)–(d) The Husimi-Q function at (a) $t = 0.1T$, (b) $t = 0.4T$, (c) $t = 0.7T$, and (d) $t = T$. (e) $\Lambda(t)$. (f) $F_Q(t)/T^2$ (blue solid line) and f_0 (red circles). $F_Q(t) = Nt^2$ for an unentangled system is represented by the blue dashed line. The shot-noise limit ($f_0 = N$) and Heisenberg limit ($f_0 = N^2$) are represented by the lower and upper black dotted lines, respectively. Parameters: $N = 100$, $\chi T = 0.1$. F_Q reaches a maximum of $28.95NT^2$, compared to $7.8NT^2$ for the OAT scheme.

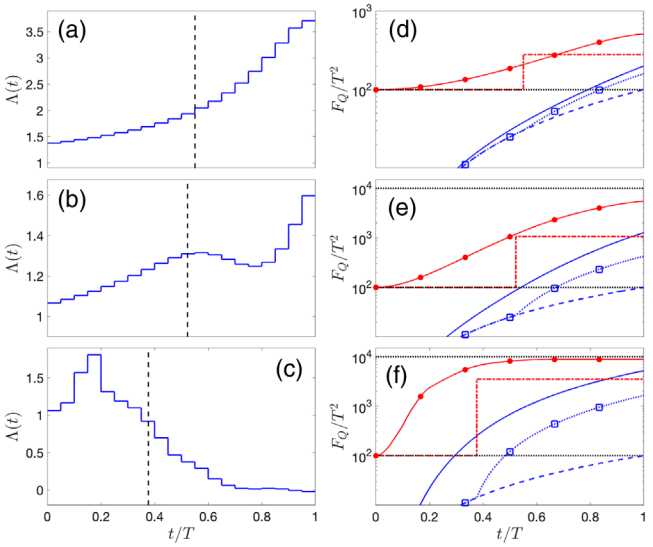

FIG. 4. Optimized scheme for different values of χT. (a)–(c) The optimum $\Lambda(t)$. The value of τ_{prep} for the optimum OAT scheme for the same parameters is indicated by the vertical dashed line. (d)–(f) $F_Q(t)$ and f_0 for our generalized scheme (blue solid line and red circles, respectively) and the optimum OAT scheme (blue squares and red dot-dashed line, respectively). The shot-noise limit ($F_Q = NT^2$ and $f_0 = N$) and Heisenberg limit ($f_0 = N^2$) are indicated by the blue dashed line and the upper and lower black dotted lines, respectively. Parameters: (a), (d) $\chi T = 0.02$, (b),(e) $\chi T = 0.06$, (c),(f) $\chi T = 0.2$. $N = 100$ was used throughout.

In traditional OAT and TNT metrology schemes, the complexity of dynamics afforded by a complicated form of $\Omega(t)$ has so far been neglected. We consider a more general class of dynamics by allowing for arbitrary choice of $\Omega(t)$ with the goal of maximizing $F_Q(T)$. We note that this is different than maximizing f_0, as rotations around $\hat{J}_x$, and subsequent dynamics, can partially overwrite the phase accumulated at earlier times [33]. Thus, there is a trade-off between maximizing the instantaneous value of $f_0(t)$, the rate of increase of $f_0(t)$, and preserving the phase accumulated at earlier times. To explore the large parameter space of possible temporal functions without restricting ourselves to solutions that correlate to simple intuitive models, we utilize machine optimization. In situations where simple solutions are in fact optimal, these will arise organically. We parametrize $\Omega(t)$ by

$$\Omega(t) = -\Lambda(t)N\frac{\chi}{2}, \tag{5}$$

where Λ is a piecewise step function. Choosing a constant $\Lambda = 1$ would correspond to TNT dynamics, but we divide the duration into 20 equal segments that are allowed to vary individually. We then evolve our initial state under the Hamiltonian (1) and use a gradient ascent algorithm with multiple, stochastically chosen starting locations to find the optimum $\Lambda(t)$ that maximizes $F_Q(T)$. Figure 3 shows the optimum $\Lambda(t)$ for $\chi T = 0.1$ and $N = 100$. We find that $F_Q(T)$ is more than a factor of 3.5 times better than the optimum OAT scheme and ~29 times better than the shot-noise limit.

We examined the optimum scheme for a range for values of χT and found different classes of behavior in different regimes (Fig. 4). For $\chi T \lesssim 0.05$, we find that the optimum behavior seems to continuously rotate the axis with increased variance into the $\hat{J}_z$ axis, which requires a larger Λ as the state becomes more sheared. For $\chi T \gtrsim 0.09$, the optimum strategy seems to be more similar to what we would traditionally think of as separate state-preparation and interrogation stages, which is to increase f_0 as much as possible early on (initially with $\Lambda \approx 1$ to initiate TNT dynamics), before increasing Λ to rotate this sensitivity into the $\hat{J}_z$ axis, and then reducing $\Lambda(t) \approx 0$ for the remainder of the evolution. In all cases, we find that using this more complicated profile for $\Lambda(t)$ significantly outperforms the traditional OAT and TNT schemes, even when τ_{prep} and θ_0 are optimized to maximize the performance.

Optimizing robustness to detection noise.—To fully extract the sensitivity from these states, we require a measurement in the $\hat{J}_x$ basis with single-particle resolution [27]. However, in some practical situations this resolution is challenging, and there is additional detection noise. We follow the convention used in [34] and model the behavior of an imperfect detector by sampling from the probability distribution

$$\tilde{P}_m(\sigma) = \sum_{m'} \Gamma_{m,m'} P_{m'}, \tag{6}$$

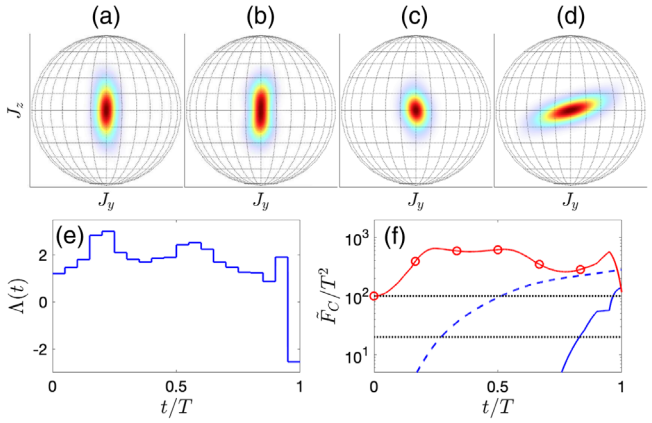

FIG. 5. Optimized scheme in the presence of detection noise. (a)–(d) The Husimi-Q function at (a) $t = 0.25T$, (b) $t = 0.5T$, (c) $t = 0.75T$, and (d) $t = T$. (e) $\Lambda(t)$. (f) $\tilde{F}_C(t)/T^2$ (blue solid line), $F_Q(t)/T^2$ (blue dashed line), and f_0 (red circles). The SNL and $\tilde{F}_C(T)$ for a CSS are indicated by the upper and lower black dotted lines, respectively. Parameters: $N = 100$, $\chi T = 0.1$, $\sigma = 10$. $\tilde{F}_C$ reaches a maximum of $\sim 1.4NT^2$.

where

$$\Gamma_{m,m'}(\sigma) = e^{-(m-m')^2/(2\sigma^2)} / \sum_m e^{-(m-m')^2/(2\sigma^2)} \tag{7}$$

convolves the raw probability distribution P_m (i.e., the result of a $\hat{J}_x$ measurement with no detection noise) with a Gaussian of width σ. The sensitivity obtainable from sampling from $\tilde{P}_m$ is then $\delta\omega^2 = 1/\tilde{F}_C$, where

$$\tilde{F}_C = \sum_m \frac{(\partial_\omega \tilde{P}_m)^2}{\tilde{P}_m} \tag{8}$$

is the classical Fisher information for this measurement. The states obtained by our optimized schemes are highly nonclassical and are very susceptible to the effects of detection noise. In fact, for the state obtained in Fig. 3, $\tilde{F}_C$ drops below the SNL for $\sigma \sim 1$.

It was found in previous work that robustness to detection noise could be drastically improved by adding an interaction-based readout (IBR), which is a period of evolution after the interrogation time, to convert the final probability distribution into one that is more robust to detection noise [24,27,35,36]. This often involves reversal of the initial state-preparation dynamics (commonly referred to as an echo) to restore the initial coherent spin state [37–45]. However, it was shown in [46] that there are schemes that perform significantly better than this. Here, we consider the time devoted to this IBR as part of our total time T and ask what is the optimum strategy in the presence of detection noise σ. Without dynamical control over the parameter χ, we cannot implement a scheme that reverses the initial state-preparation dynamics. However, it is possible that appropriate manipulation of $\Lambda(t)$ may approximate echo dynamics. We approach this by replacing F_Q with $\tilde{F}_C$ as the metric in our optimization algorithm. However, as in [27], we found that the performance could be significantly improved by adding one additional parameter, which is a small phase offset before the final measurement; that is, $|\Psi(T)\rangle \to \exp(i\phi\hat{J}_z)|\Psi(T)\rangle$ and optimize over the parameter ϕ.

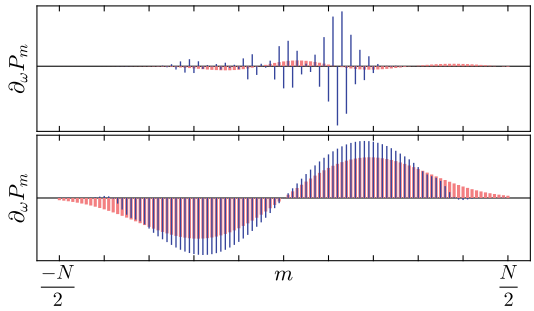

FIG. 6. Susceptibility of the final probability distribution to detection noise. $\partial_\omega P_m$ (narrow blue bars) and $\partial_\omega \tilde{P}_m$ (wide pink bars) for the scheme illustrated in Figs. 3 (top) and 5 (bottom). (Top) $\partial_\omega \tilde{P}_m$ has been multiplied by 500 in order for it to be displayed on the same scale.

Figure 5 shows $\tilde{F}_C$ and the optimum shape of $\Lambda(t)$ for $\sigma = \sqrt{N}$, which represents a level of detection noise that usually reduces sensitivity to worse than the SNL [46]. We see that, while the early part of the scheme is still concerned with maximizing f_0, the later part is attempting to restore the state to one that is less susceptible to detection noise. The final value of $\tilde{F}_C \approx 1.4NT^2$ is considerably better than the SNL. For this value of σ, a CSS results in a sensitivity $\tilde{F}_C \approx 0.2NT^2$. We note that, instead of restoring to something approximating a CSS, the final distribution is antisqueezed in $\hat{J}_x$, which was shown to provide greater robustness to detection noise [3,27,46].

By looking at the form of $\partial_\omega P_m$ and $\partial_\omega \tilde{P}_m$ (Fig. 6), we can see how this dynamics has increased the sensitivity in the presence of detection noise when compared to the scheme illustrated in Fig. 3. In the scheme optimized without noise, the final state results in a probability distribution where $\partial_\omega P_m$ for neighboring m alternates in sign and so are washed out by detection noise of order $\sigma \sim 1$. When we optimize in the presence of detection noise, the scheme results in a final probability distribution where a small change in ω simply results in a shift in the mean, which is only minimally effected by noise less than the width of the distribution.

Discussion.—Hayes *et al.* [31] also considered the use of traditional OAT dynamics concurrently with interrogation and found that sensitivities significantly better than the SNL were possible. Comparing our scheme to the scheme of Hayes *et al.*, for equivalent parameters ($N = 100, \chi T = 0.5$), we find a sensitivity ~ 7.2 times better, while for $\chi T = 0.04$,

our scheme achieves a sensitivity ∼5.5 times better than the SNL, while they find no improvement over the SNL. Our scheme also outperforms TNT dynamics.

The scheme presented in this Letter is an example of a machine-designed sensor, where instead of adhering to traditional sensing intuition (i.e., separate state-preparation and interrogation stages), we simply optimized the controllable parameters of the system using the final sensitivity as the appropriate metric. This approach frees us from the existing paradigm of state preparation followed by interrogation, which is the philosophy utilized by all quantum-enhanced atomic sensing experiments so far demonstrated. The significant increase in performance that this approach provides indicates the power of this technique and could be used in other quantum-enhanced sensing protocols that involve the use of a controllable dynamic parameter, such as when coherent coupling pulses are used to increase the entangled population spontaneously generated from spin-changing collisions [41,47,48], four-wave mixing [49], or Raman superradiance [50,51]. Finally, we note that, while this scheme is capable of enhancing the sensitivity of atomic clocks and magnetometers, the continuous use of coupling pulses is incompatible with atomic gravimeters and accelerometers due to the requirement of space-time separated modes [1,52]. However, this scheme could be useful in a Halkyard-Jones-Gardiner rotation sensor, due to the ability to continuously couple the constantly overlapping counterrotating modes [53,54].

We acknowledge fruitful discussions with Luca Pezze, Augusto Smerzi, Manuel Gessner, Jacob Dunningham, and Alex Radcliffe.

*simon.a.haine@gmail.com

[1] A. D. Cronin, J. Schmiedmayer, and D. E. Pritchard, Optics and interferometry with atoms and molecules, Rev. Mod. Phys. **81**, 1051 (2009).
[2] L. Pezze, A. Smerzi, M. K. Oberthaler, R. Schmied, and P. Treutlein, Quantum metrology with nonclassical states of atomic ensembles, Rev. Mod. Phys. **90**, 035005 (2018).
[3] O. Hosten, N. J. Engelsen, R. Krishnakumar, and M. A. Kasevich, Measurement noise 100 times lower than the quantum-projection limit using entangled atoms, Nature (London) **529**, 505 (2016).
[4] H. A. Rabitz, M. M. Hsieh, and C. M. Rosenthal, Quantum optimally controlled transition landscapes, Science **303**, 1998 (2004).
[5] M. Kitagawa and M. Ueda, Squeezed spin states, Phys. Rev. A **47**, 5138 (1993).
[6] K. Mølmer and A. Sørensen, Multiparticle Entanglement of Hot Trapped Ions, Phys. Rev. Lett. **82**, 1835 (1999).
[7] J. Esteve, C. Gross, A. Weller, S. Giovanazzi, and M. K. Oberthaler, Squeezing and entanglement in a Bose-Einstein condensate, Nature (London) **455**, 1216 (2008).
[8] Y. Li, P. Treutlein, J. Reichel, and A. Sinatra, Spin squeezing in a bimodal condensate: Spatial dynamics and particle losses, Eur. Phys. J. B **68**, 365 (2009).
[9] S. A. Haine and M. T. Johnsson, Dynamic scheme for generating number squeezing in Bose-Einstein condensates through nonlinear interactions, Phys. Rev. A **80**, 023611 (2009).
[10] I. D. Leroux, M. H. Schleier-Smith, and V. Vuletić, Implementation of Cavity Squeezing of a Collective Atomic Spin, Phys. Rev. Lett. **104**, 073602 (2010).
[11] C. Gross, T. Zibold, E. Nicklas, J. Esteve, and M. K. Oberthaler, Nonlinear atom interferometer surpasses classical precision limit, Nature (London) **464**, 1165 (2010).
[12] M. F. Riedel, P. Böhi, Y. Li, T. W. Hänsch, A. Sinatra, and P. Treutlein, Atom-chip-based generation of entanglement for quantum metrology, Nature (London) **464**, 1170 (2010).
[13] W. Muessel, H. Strobel, D. Linnemann, D. B. Hume, and M. K. Oberthaler, Scalable Spin Squeezing for Quantum-Enhanced Magnetometry with Bose-Einstein Condensates, Phys. Rev. Lett. **113**, 103004 (2014).
[14] S. A. Haine, J. Lau, R. P. Anderson, and M. T. Johnsson, Self-induced spatial dynamics to enhance spin squeezing via one-axis twisting in a two-component Bose-Einstein condensate, Phys. Rev. A **90**, 023613 (2014).
[15] S. P. Nolan and S. A. Haine, Generating macroscopic superpositions with interacting Bose-Einstein condensates: Multimode speedups and speed limits, Phys. Rev. A **98**, 063606 (2018).
[16] B. Yurke, S. L. McCall, and J. R. Klauder, SU(2) and SU(1,1) interferometers, Phys. Rev. A **33**, 4033 (1986).
[17] G. Tóth, Multipartite entanglement and high-precision metrology, Phys. Rev. A **85**, 022322 (2012).
[18] P. Hyllus, W. Laskowski, R. Krischek, C. Schwemmer, W. Wieczorek, H. Weinfurter, L. Pezzé, and A. Smerzi, Fisher information and multiparticle entanglement, Phys. Rev. A **85**, 022321 (2012).
[19] P. Hauke, M. Heyl, L. Tagliacozzo, and P. Zoller, Measuring multipartite entanglement through dynamic susceptibilities, Nat. Phys. **12**, 778 (2016).
[20] A. Micheli, D. Jaksch, J. I. Cirac, and P. Zoller, Many-particle entanglement in two-component Bose-Einstein condensates, Phys. Rev. A **67**, 013607 (2003).
[21] H. Strobel, W. Muessel, D. Linnemann, T. Zibold, D. B. Hume, L. Pezzè, A. Smerzi, and M. K. Oberthaler, Fisher information and entanglement of non-Gaussian spin states, Science **345**, 424 (2014).
[22] W. Muessel, H. Strobel, D. Linnemann, T. Zibold, B. Julia-Diaz, and M. K. Oberthaler, Twist-and-turn spin squeezing in Bose-Einstein condensates, Phys. Rev. A **92**, 023603 (2015).
[23] G. Sorelli, M. Gessner, A. Smerzi, and L. Pezzè, Fast and optimal generation of entanglement in bosonic Josephson junctions, Phys. Rev. A **99**, 022329 (2019).
[24] S. S. Mirkhalaf, S. P. Nolan, and S. A. Haine, Robustifying twist-and-turn entanglement with interaction-based readout, Phys. Rev. A **97**, 053618 (2018).
[25] G. Tóth and I. Apellaniz, Quantum metrology from a quantum information science perspective, J. Phys. A **47**, 424006 (2014).

[26] R. Demkowicz-Dobrzanski, M. Jarzyna, and J. Kolodynski, Quantum limits in optical interferometry, Prog. Opt. **60**, 345 (2015).
[27] S. P. Nolan, S. S. Szigeti, and S. A. Haine, Optimal and Robust Quantum Metrology Using Interaction-Based Readouts, Phys. Rev. Lett. **119**, 193601 (2017).
[28] F. T. Arecchi, E. Courtens, R. Gilmore, and H. Thomas, Atomic coherent states in quantum optics, Phys. Rev. A **6**, 2211 (1972).
[29] D. J. Wineland, J. J. Bollinger, W. M. Itano, F. L. Moore, and D. J. Heinzen, Spin squeezing and reduced quantum noise in spectroscopy, Phys. Rev. A **46**, R6797 (1992).
[30] In practice, $\Omega(t)$ is a very short temporal pulse with a characteristic timescale much shorter than the timescale for dynamics caused by the other terms in the Hamiltonian, with $\int \Omega(t)dt = \theta_0$.
[31] A. J. Hayes, S. Dooley, W. J. Munro, K. Nemoto, and J. Dunningham, Making the most of time in quantum metrology: concurrent state preparation and sensing, Quantum Sci. Technol. **3**, 035007 (2018).
[32] Hayes *et al.* [31] used a slightly different Hamiltonian $\hat{H} = \hbar\chi\hat{J}_x^2 + \hbar\omega\hat{J}_y$ and therefore did not need this additional rotation.
[33] S. A. Haine, Quantum noise in bright soliton matterwave interferometry, New J. Phys. **20**, 033009 (2018).
[34] L. Pezzé and A. Smerzi, Ultra Sensitive Two-Mode Interferometry with Single-Mode Number Squeezing, Phys. Rev. Lett. **110**, 163604 (2013).
[35] O. Hosten, R. Krishnakumar, N. J. Engelsen, and M. A. Kasevich, Quantum phase magnification, Science **352**, 1552 (2016).
[36] F. Fröwis, P. Sekatski, and W. Dür, Detecting Large Quantum Fisher Information with Finite Measurement Precision, Phys. Rev. Lett. **116**, 090801 (2016).
[37] M. Gabbrielli, L. Pezzè, and A. Smerzi, Spin-Mixing Interferometry with Bose-Einstein Condensates, Phys. Rev. Lett. **115**, 163002 (2015).
[38] E. Davis, G. Bentsen, and M. Schleier-Smith, Approaching the Heisenberg Limit Without Single-Particle Detection, Phys. Rev. Lett. **116**, 053601 (2016).
[39] T. Macrì, A. Smerzi, and L. Pezzè, Loschmidt echo for quantum metrology, Phys. Rev. A **94**, 010102(R) (2016).
[40] D. Linnemann, H. Strobel, W. Muessel, J. Schulz, R. J. Lewis-Swan, K. V. Kheruntsyan, and M. K. Oberthaler, Quantum-Enhanced Sensing Based on Time Reversal of Nonlinear Dynamics, Phys. Rev. Lett. **117**, 013001 (2016).
[41] S. S. Szigeti, R. J. Lewis-Swan, and S. A. Haine, Pumped-Up SU(1,1) Interferometry, Phys. Rev. Lett. **118**, 150401 (2017).
[42] R. Fang, R. Sarkar, and S. Shahriar, Enhancing sensitivity of an atom interferometer to the Heisenberg limit using increased quantum noise, arXiv:1707.08260.
[43] F. Anders, L. Pezzè, A. Smerzi, and C. Klempt, Phase magnification by two-axis countertwisting for detection-noise robust interferometry, Phys. Rev. A **97**, 043813 (2018).
[44] J. Huang, M. Zhuang, and C. Lee, Non-Gaussian precision metrology via driving through quantum phase transitions, Phys. Rev. A **97**, 032116 (2018).
[45] R. J. Lewis-Swan, M. A. Norcia, J. R. K. Cline, J. K. Thompson, and A. M. Rey, Robust Spin Squeezing Via Photon-Mediated Interactions on an Optical Clock Transition, Phys. Rev. Lett. **121**, 070403 (2018).
[46] S. A. Haine, Using interaction-based readouts to approach the ultimate limit of detection-noise robustness for quantum-enhanced metrology in collective spin systems, Phys. Rev. A **98**, 030303(R) (2018).
[47] I. Kruse, K. Lange, J. Peise, B. Lücke, L. Pezzè, J. Arlt, W. Ertmer, C. Lisdat, L. Santos, A. Smerzi, and C. Klempt, Improvement of an Atomic Clock Using Squeezed Vacuum, Phys. Rev. Lett. **117**, 143004 (2016).
[48] S. P. Nolan, J. Sabbatini, M. W. J. Bromley, M. J. Davis, and S. A. Haine, Quantum enhanced measurement of rotations with a spin-1 Bose-Einstein condensate in a ring trap, Phys. Rev. A **93**, 023616 (2016).
[49] S. A. Haine and A. J. Ferris, Surpassing the standard quantum limit in an atom interferometer with four-mode entanglement produced from four-wave mixing, Phys. Rev. A **84**, 043624 (2011).
[50] S. A. Haine, Information-Recycling Beam Splitters for Quantum Enhanced Atom Interferometry, Phys. Rev. Lett. **110**, 053002 (2013).
[51] S. A. Haine and W. Y. Sarah Lau, Generation of atom-light entanglement in an optical cavity for quantum enhanced atom interferometry, Phys. Rev. A **93**, 023607 (2016).
[52] M. Kritsotakis, S. S. Szigeti, J. A. Dunningham, and S. A. Haine, Optimal matter-wave gravimetry, Phys. Rev. A **98**, 023629 (2018).
[53] P. L. Halkyard, M. P. A. Jones, and S. A. Gardiner, Rotational response of two-component Bose-Einstein condensates in ring traps, Phys. Rev. A **81**, 061602(R) (2010).
[54] S. A. Haine, Mean-Field Dynamics and Fisher Information in Matter Wave Interferometry, Phys. Rev. Lett. **116**, 230404 (2016).